



Low thrust Earth–Moon transfer trajectories via lunar capture set

Yongfei Gao¹ · Zhaokui Wang² · Yulin Zhang^{1,2}

Received: 14 December 2018 / Accepted: 2 December 2019 / Published online: 9 December 2019
© Springer Nature B.V. 2019

Abstract A cislunar cargo spacecraft with low-thrust propulsion traveling between the Earth and the Moon is essential for sustainable, long-term manned lunar exploration. In low-thrust Earth–Moon transfer (LTEMT), lunar capture is the primary prerequisite for spacecraft subject to the circular restricted three-body model. Therefore, this study identifies sufficient conditions for lunar capture, which are determined by the Jacobi integral and Hill’s region. This paper proposes a guidance scheme that includes thrust direction, thrust efficiency, and a five-stage flight control sequence based on the variation of the Jacobi integral. The LTEMT problem is then converted to an initial value problem of a differential equation with three parameters. Lunar capture set theories (LCSTs), which are convenient for identifying lunar capture sets, are presented and proved according to the continuous properties of the ordinary differential equation. Finally, the solutions of the LTEMT trajectories departing from a geosynchronous orbit with an altitude of approximately 35,827 km are discussed for different thrust accelerations and cut-off values of the thrust efficiency. The robustness is analyzed assuming that navigation and switching time errors are present to demonstrate the adaptability of this method. The results reveal that the proposed guidance scheme and LCSTs can provide technical support for future cislunar cargo missions.

Keywords Cargo spacecraft · Low thrust · Earth–Moon transfer · Lunar capture set theory · Jacobi integral

✉ Z. Wang
wangzk@tsinghua.edu.cn

¹ College of Aerospace Science and Engineering, National University of Defense Technology, Changsha 410073, China

² School of Aerospace Engineering, Tsinghua University, Beijing 100084, China

1 Introduction

Manned lunar exploration has become the central concern of various space powers (Crusan et al. 2018) such as China, the United States, and the European Union. In previous studies, manned spacecraft transfer trajectories, i.e., two-impulse direct transfer trajectories between the Earth and a lunar orbital station, have been solved (Gao et al. 2018). In addition to a manned spacecraft, a cargo spacecraft for supply deliveries between the Earth and the Moon (Mammarella et al. 2019; Woolley et al. 2019) is essential for sustainable long-term manned lunar exploration (Hoffman et al. 2011). In cargo spacecraft, a higher load ratio results in higher efficiency and lower cost. Owing to the substantial flight times of cargo spacecraft, an electric or nuclear propulsion system with a high specific impulse of several thousand seconds is an ideal choice (Mercer et al. 2016; McGuire et al. 2017). However, designing low-thrust trajectories is challenging, particularly for low-thrust Earth–Moon transfer (LTEMT), where multibody dynamics are important, and the solutions involve multiple revolutions (Oshima and Campagnola 2017). Computing the long-duration thrust vector histories and ensuring that the cargo spacecraft is captured by the Moon are the main difficulties in designing LTEMT trajectories.

Typically, the design of a low-thrust transfer trajectory is modeled as a calculus of variations problem that maximizes or minimizes a performance index such as the spacecraft’s final mass or total flight time. Methods of solving these problems can be classified as indirect, direct (Betts 1998), and hybrid methods. In the indirect method, Pontryagin’s principle is used to obtain a two-point boundary value problem (TPBVP) and the necessary optimal conditions from the calculus of variations formulation. The TPBVP can be solved by finding the unknown initial costate variables.

The direct method converts the calculus of variations problem into a nonlinear optimization problem in which nonlinear programming is employed to minimize the performance index. The entire trajectory is represented in terms of nodes, and many design variables are used to increase the convergence radius (Graham and Rao 2015, 2016). The hybrid method uses the necessary conditions from optimal control theory to parameterize the thrust vector histories. Direct maximization replaces the indirect solution of the transversality conditions (Kluever and Pierson 1995; Ozimek and Howell 2010).

In contrast to the direct and hybrid methods, the indirect method requires solution of the TPBVP for optimal control; a disadvantage of the method is a small radius of convergence. Estimation of the initial costates (Lee et al. 2009, 2012) is particularly difficult owing to the long-duration transfer and multiple revolutions. Pérez-Palau and Epenoy (2018) investigated minimum-fuel low-thrust transfers between low Earth orbit and low lunar orbit (LLO) assuming that an initial velocity increment is provided to the spacecraft. Oshima and Campagnola (2017) searched globally for low-thrust transfers to the Moon in the planar circular restricted three-body problem (CRTBP) by reducing the dimensions of the initial costate set. The homotopy method is often applied to overcome the disadvantages of solving low-thrust trajectory optimization problems such as minimum-fuel (Haberkorn and Martinon 2004; Caillau et al. 2012; Jiang 2012; Zhang et al. 2015; Chi et al. 2017, 2018) and minimum-time low-thrust orbital transfers (Pan et al. 2018).

For the direct and hybrid methods, it is necessary to supply an initial approximation because these methods are nonlinear optimization algorithms. A simple linear function between boundary conditions is not applicable to LTEMTs because the dynamics are nonlinear, the problem is large, and there are many local solutions (Betts and Erb 2003). Typically, a three-stage approach consisting of an Earth-escape spiral followed by a translunar coast arc and then a Moon-capture spiral to the desired LLO is used. The preliminary LTEMt trajectories are obtained by dividing the entire trajectory into segments and connecting these segments to each other by constructing equality constraints at the boundaries of each segment (Kluever and Pierson 1995; Gao 2007). Herman and Conway (1998) computed the initial values using a trajectory that did not consider boundary conditions, and the method was applied to obtain a solution that could easily yield an LTEMt with an initial low-thrust acceleration greater than 10^{-3} m/s^2 . Betts and Erb (2003) proposed a four-step procedure to construct the initial guess based on the three-stage approach and presented an LTEMt trajectory that requires the solution of a sparse optimization problem with 211,031 variables and 146,285 constraints. Song and Park (2009) used analytically optimized Earth-escape

and Moon-capture segments and a numerical optimization method to match the spacecraft's states and establish a final near-optimal trajectory.

The shape-based trajectory design method (Petropoulos and Longuski 2004) is another technique for designing preliminary low-thrust trajectories. In this method, the shape of the trajectory is assumed to have the form of a specific function, and the boundary conditions are used to compute a few of the unknown parameters of the assumed fixed function. Finite Fourier series have been implemented for low-thrust trajectory approximations, and the capability was demonstrated by generating planar Earth–Moon transfer (Taheri and Abdelkhalik 2015) and three-dimensional interplanetary transfer trajectories (Taheri and Abdelkhalik 2016; Taheri and Kolmanovsky 2018).

Although previous research has produced LTEMt trajectories satisfying the boundary and dynamics constraints, the lunar capture problem, the solution of which ensures that a cargo spacecraft is captured by the Moon, has not been solved. Ensuring that the spacecraft enters Moon orbit under a preset guidance law is very important for engineering implementations. Furthermore, considering Earth–Moon transfer, lunar capture is a prerequisite and a core issue for any propulsion system. For chemical propulsion, the spacecraft is positioned in LLO by lunar orbital injection (LOI). Unlike chemical propulsion systems, an electric propulsion system cannot apply an instantaneous LOI to achieve lunar capture. Therefore, this study focuses on lunar capture. Once the spacecraft has entered the lunar capture orbit, the LTEMt problem is transformed into a lunar orbit transfer problem, which can be solved by feedback control (Jagannatha et al. 2018).

This paper is organized as follows. The controlled CRTBP is described in Sect. 2 and used to derive the sufficient conditions for lunar capture in Sect. 3. A guidance scheme for the LTEMt is then proposed. Under the guidance scheme, the design of the LTEMt trajectories is converted to an initial value problem of a differential equation with three parameters. On the basis of the continuous dependence properties of the differential equation, lunar capture set theories (LCSTs) are proposed and proved in Sect. 4. LTEMt trajectories for different thrust accelerations and thrust efficiencies are presented in Sect. 5. Finally, robustness analysis considering navigation and switching time errors shows that the proposed method can provide technical support for future cislunar cargo spacecraft.

2 Controlled circular restricted three-body problem

In the CRTBP, two primary bodies P_1 and P_2 with masses m_1 and m_2 , respectively ($m_1 > m_2 > 0$) move under mutual gravity in circular orbits about their common center of

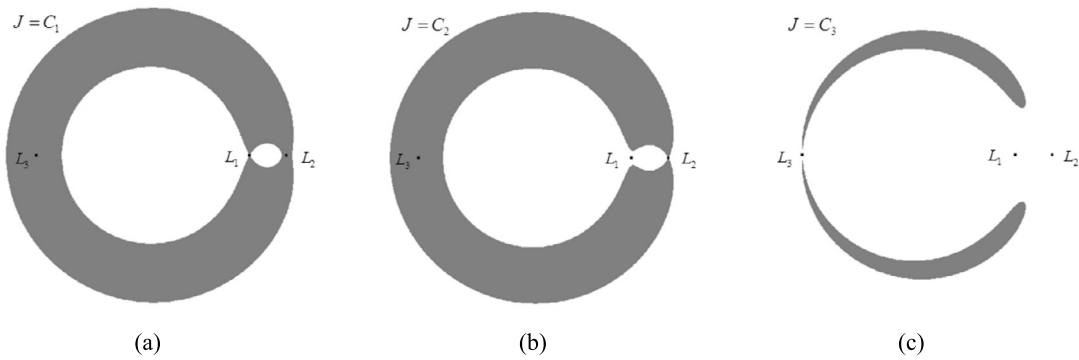


Fig. 1 Hill’s region for (a) $J = C_1$, (b) $J = C_2$, and (c) $J = C_3$

Table 1 Normalization constants

Physical constant	Value
Mass parameter μ	1.2150568×10^{-2}
Distance unit (LU)	3.84405×10^8 m
Time unit (TU)	3.75676967×10^5 s
Speed unit (VU)	1.02323×10^3 m/s

mass. A third body P , which is assumed to have infinitesimal mass, moves under the gravity of the primaries. The motion of the primaries is not affected by P . Here, P represents a spacecraft, and P_1, P_2 represent the Earth and the Moon, respectively. The standard canonical system of units associated with this model is used. $\mu = m_2/(m_1 + m_2)$ denotes the mass parameter. The distance, velocity, and time units are listed in Table 1.

For low-thrust propulsion, the dynamics equation in the Earth–Moon rotating frame can be written as

$$\dot{s} = f(s) + g(u, \alpha, m)$$

$$\Rightarrow \begin{bmatrix} \dot{r} \\ \dot{v} \\ \dot{m} \end{bmatrix} = \begin{bmatrix} v \\ h(v) + \Omega_r \\ 0_{3 \times 1} \end{bmatrix} + \begin{bmatrix} 0_{3 \times 1} \\ u \frac{T_{\max}}{m} \alpha \\ -u \frac{T_{\max}}{c} \end{bmatrix} \quad (1)$$

where $s = (r^T, v^T, m)$ is the state vector of the spacecraft; $r = [x, y, z]^T$ and $v = [\dot{x}, \dot{y}, \dot{z}]^T$ are the position and velocity vectors in the Earth–Moon rotating frame, respectively; and m represents the mass of the spacecraft, which has an initial value of $m_0 = 1$. The control variables include the throttle factor $u \in [0, 1]$ and thrust direction unit vector α . T_{\max} denotes the maximum thrust magnitude; $c = I_{sp}g_0$ is the exhaust velocity, where I_{sp} and g_0 are the thruster specific impulse and gravitational acceleration at sea level, respectively. Therefore, when $u = 0$,

$$\dot{s} = f(s) \quad (2)$$

is the dynamics equation of the CRTBP.

The function $h(v)$ is defined as

$$h(v) = \begin{bmatrix} 2\dot{y} \\ -2\dot{x} \\ 0 \end{bmatrix} \quad (3)$$

Ω is the effective potential

$$\Omega = \Omega(r)$$

$$= \frac{1}{2}(x^2 + y^2) + \frac{1}{2}\mu(1 - \mu) + \frac{\mu}{r_2} + \frac{1 - \mu}{r_1} \quad (4)$$

with

$$r_1 = \sqrt{(x + \mu)^2 + y^2 + z^2} \quad \text{and}$$

$$r_2 = \sqrt{(x - 1 + \mu)^2 + y^2 + z^2},$$

as P_1 and P_2 are located at $(-\mu, 0), (1 - \mu, 0)$, respectively. The term Ω_r is the partial derivative of Ω with respect to r .

The system of differential equations in (2) contains three collinear points, denoted as $L_i, i = 1, 2, 3$, on the x axis of the Earth–Moon rotating frame and allows for an integral of motion, called the Jacobi integral J :

$$J = 2\Omega - v^2 \quad (5)$$

the value of which is determined from the initial conditions and is used as a measure of energy. Here, $v = \|v\|$ is the velocity in the Earth–Moon rotating frame. For lower values of J , the energy of the spacecraft is higher. Substituting $v = 0$ in Eq. (5) for a given value of J defines the boundary of Hill’s region, in which the spacecraft is energetically permitted to move, as shown in Fig. 1.

In Fig. 1, $C_i, i = 1, 2, 3$, are the values of the Jacobi integral at points $L_i, i = 1, 2, 3$, which satisfy the condition $C_1 > C_2 > C_3$. Table 2 lists the locations and Jacobi integrals of the collinear points $L_i, i = 1, 2, 3$. As shown in Fig. 1(a), for $J < C_1$, motion between the Earth and the Moon is feasible (Mengali and Quarta 2005).

Table 2 Locations and Jacobi integrals of the collinear points $L_i, i = 1, 2, 3$

	L_1	L_2	L_3
$x _{L_i}$ (LU)	0.837367772	1.155270268	-1.005062638
C_i	3.200343883	3.184163250	3.024150064

Note that the state vectors and dynamics equation given above are discussed in the Earth–Moon rotating frame. It is necessary to understand the relationship between the state vector $s = [r^T, v^T, m]^T$ in the Earth–Moon rotating frame and $S = [R^T, V^T, m]^T$ in the Earth-centered inertial frame.

$$\begin{cases} \dot{r} = M_z(t)R - [\mu, 0, 0]^T \\ \dot{v} = M_z(t)V + M'_z(t)R \end{cases} \quad (6)$$

where M_z and M'_z are the rotation matrix and its derivative, respectively. $R = [X, Y, Z]^T$ and $V = [\dot{X}, \dot{Y}, \dot{Z}]^T$ are the normalized position and velocity vectors in the Earth-centered inertial frame, respectively. In addition, t is the normalized time associated with the state $s = [r^T, v^T, m]^T$.

3 Lunar capture conditions and the guidance law

3.1 Lunar capture conditions

The cargo spacecraft is initially in an Earth parking orbit with the Jacobi integral $J_0 > C_1$. Under continuous low thrust, the altitude of the spacecraft increases and the Jacobi integral $J(t)$ of the transfer trajectory decreases until $J = C_1$. At this time, although the spacecraft reaches the critical condition for Earth–Moon transfer, it may not be able to cross the point L_1 to the near-Moon space because its altitude is too low. Therefore, the spacecraft continues to accelerate, and this minimum Jacobi integral is denoted as J_{\min} . When the transfer trajectory can reach the near-Moon space, deceleration thrust is applied from the appropriate time until $J = C_1$. At this time, the state of the spacecraft may be in three regions described by Eqs. (7)–(9), which are separated by $R = x|_{L_1}$ and $R = x|_{L_2}$, as shown in Fig. 2.

$$I: \{(x, y) | R < x|_{L_1} \& J = C_1\} \quad (7)$$

$$II: \{(x, y) | x|_{L_1} < R < x|_{L_2} \& J = C_1\} \quad (8)$$

$$III: \{(x, y) | R > x|_{L_2} \& J = C_1\} \quad (9)$$

where $R = \sqrt{x^2 + y^2}$.

If the terminal state is located in II, which satisfies the following conditions,

$$\begin{cases} J_f = C_1 \\ x|_{L_1} < R_f < x|_{L_2} \end{cases} \quad (10)$$

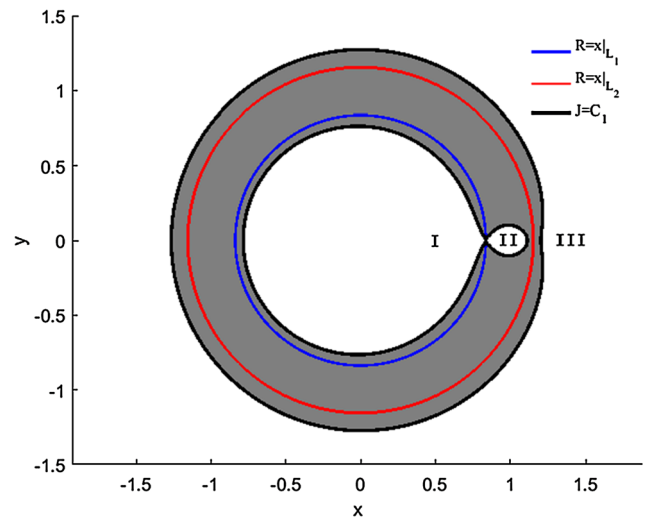


Fig. 2 Three areas separated by $R = x|_{L_1}$ and $R = x|_{L_2}$ in Hill’s region $J = C_1$

the spacecraft has been captured by the Moon. Here, the subscript f denotes the terminal state of the transfer trajectory. Therefore, Eq. (10) represents the sufficient condition for lunar capture.

3.2 Thrust direction

Let the Jacobi integral of the initial state s_0 be $J_0 = J(T_0)$, where T_0 is the initial epoch. Regarding the dynamics equation in Eq. (1),

$$\dot{v} = h(v) + \Omega_r + u \frac{T_{\max}}{m} \alpha \quad (11)$$

We multiply Eq. (11) by v and obtain the resulting sum. The result, in combination with Eq. (5), can be written as

$$\frac{dJ}{dt} = -u \frac{2T_{\max}}{m} (\alpha \cdot v) \quad (12)$$

The rate of change of the Jacobi integral is related to the thrust acceleration and the dot product $\alpha \cdot v$. Therefore, when $\alpha = \pm v/v$, that is, the direction of the thrust is the same as or opposite to the direction of the velocity, the value of $|dJ/dt|$ is maximum.

$$\frac{dJ}{dt} = \mp u \frac{2T_{\max}}{m} v \quad (13)$$

Integrating Eq. (13) yields Eq. (14).

$$J(t) - J_0 = \mp \int_{T_0}^t u \frac{2T_{\max}}{m} v dt \quad (14)$$

Here, \mp corresponds to $\alpha = \pm v/v$.

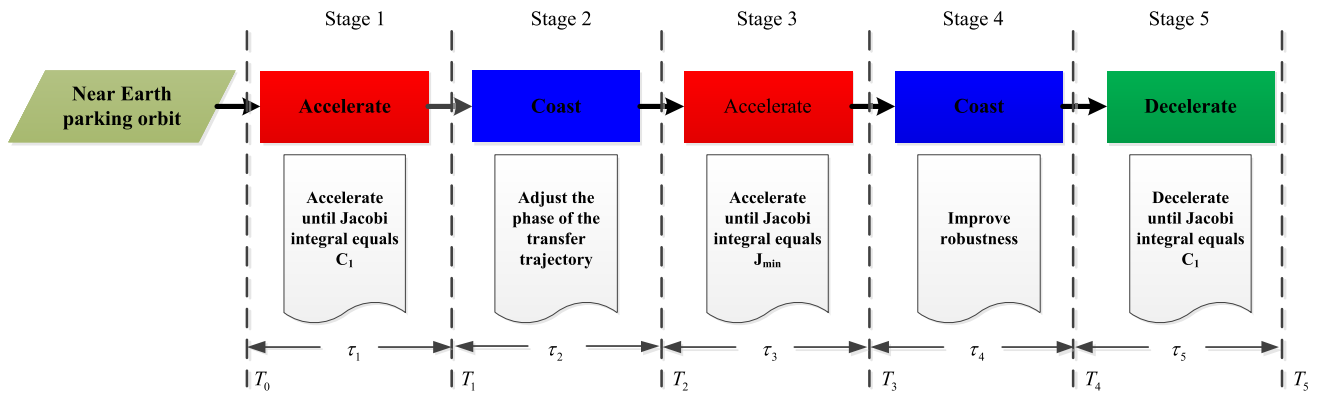


Fig. 3 Flight control sequence for LTEM spacecraft departing from near-Earth parking orbit

3.3 Thrust efficiency

At time t_0 , for state $s_0 = (r_0^T, v_0^T, m_0)^T$, although the thrust direction $\alpha_0 = v_0 / \|v_0\|$ ensures the maximum change in the Jacobi integral at the current position, it does not provide any information about the thrust’s effectiveness as compared with that at other locations in the same revolution. For example, for another state s_1 in the same revolution $\varphi(s_0)$, evaluating the efficiency of these two thrusts is a problem. Here, the revolution $\varphi(s_0)$ is defined as

$$\varphi(s_0) : \begin{cases} \dot{s} = f(s) \\ s(t_0) = s_0, \end{cases} \quad t_0 \leq t \leq t_0 + T \quad (15)$$

where T is the orbital period of the revolution.

As the variation in the Jacobi integral during the transfer is related to the velocity, as shown in Eq. (13), it is natural to define the thrust efficiency in state s as

$$\eta(s) = \frac{v - v_{\min}}{v_{\max} - v_{\min}} \quad (16)$$

where

$$v_{\min} = \min\{v|\varphi(s)\} \quad (17)$$

$$v_{\max} = \max\{v|\varphi(s)\} \quad (18)$$

are the minimum and maximum velocities in the same revolution $\varphi(s)$, respectively.

Considering two states s_0 and s_1 in the same revolution, if $\eta(s_0) > \eta(s_1)$, the thrust in state s_0 produces a larger change in the Jacobi integral than the thrust in state s_1 . Thus, fuel can be conserved by choosing to apply thrust in states with higher thrust efficiency. Therefore, a cut-off value $\eta_{cut} \in [0, 1)$ is chosen to prevent the spacecraft from thrusting if the efficiency is below this value. That is,

$$u(t) = \begin{cases} 1, & \eta > \eta_{cut} \\ 0, & \eta < \eta_{cut} \end{cases} \quad (19)$$

For $\eta_{cut} = 0$, the propulsion system is powered on during the transfer. A larger cut-off value is expected to result in greater propellant savings but a longer flight time.

To avoid numerical integration of Eq. (15) and improve the computational efficiency, the velocity vector v in Eqs. (17) and (18) can be calculated using Eq. (6).

$$v = \begin{bmatrix} \cos t & \sin t & 0 \\ -\sin t & \cos t & 0 \\ 0 & 0 & 1 \end{bmatrix} V + \begin{bmatrix} -\sin t & \cos t & 0 \\ -\cos t & -\sin t & 0 \\ 0 & 0 & 0 \end{bmatrix} R \quad (20)$$

Then, the velocity v in Eqs. (17) and (18) is written as

$$v = \|v\| = \sqrt{(X - \dot{Y})^2 + (Y + \dot{X})^2 + \dot{Z}^2} \quad (21)$$

Here, $R = [X, Y, Z]^T$ and $V = [\dot{X}, \dot{Y}, \dot{Z}]^T$ can be analytically approximated by the values from the two-body problem.

3.4 Flight control sequence

As shown in Fig. 3, a spacecraft departing from a near-Earth parking orbit passes through five flight stages until $J_f = C_1$, where τ_i ($i = 1, \dots, 5$) is the duration of each stage. T_i ($i = 1, \dots, 5$) is the terminal time of each stage, which satisfies $T_i = T_{i-1} + \tau_i$ ($i = 1, \dots, 5$) and $T_f = T_5$.

Stage 1: This stage is used to accumulate energy for the spacecraft. The spacecraft is accelerated to the state in which the Jacobi integral equals C_1 . The flight time of this stage accounts for a majority of the total flight time. Hence, the thrust efficiency in this stage is a critical factor affecting the fuel consumption of the LTEM. Therefore, η_{cut} is defined in Stage 1, and the flight time τ_1 satisfies

$$C_1 - J_0 = - \int_{T_0}^{T_0 + \tau_1} u \frac{2T_{\max}}{m} v dt \quad (22)$$

where the throttle factor during $[T_0, T_1]$ satisfies Eq. (19). The additional computational load during the integration due to the analytical expression of the thrust efficiency is minor.

Stage 2: This stage is used to adjust the phase of the transfer trajectory such that the phase relative to the x axis of the Earth–Moon rotating frame satisfies the condition that the spacecraft can cross the near- L_1 space. During this stage, the propulsion system is powered off; thus, $u(t) = 0, T_1 \leq t \leq T_2$, and $J(t) = C_1$. The flight time τ_2 is related to the initial state s_0 and thrust acceleration T_{\max}/m .

Stage 3: The acceleration in the first stage changes the Jacobi integral of the spacecraft to C_1 . At this time, the spacecraft cannot cross the near- L_1 space and enter lunar space, as shown in Fig. 1(a). In Stage 3, the spacecraft is accelerated such that the Jacobi integral equals J_{\min} , which satisfies $J_{\min} < C_1$. During this stage, the propulsion system is powered on; namely, $u(t) = 1, T_2 \leq t \leq T_3$. The thrust direction is $\alpha = v/\|v\|$, and the flight time τ_3 satisfies

$$J_{\min} - C_1 = - \int_{T_2}^{T_2+\tau_3} \frac{2T_{\max}}{m} v dt \tag{23}$$

Here, J_{\min} is the minimum Jacobi integral of the LTEM trajectory, and τ_3 is an undetermined parameter.

Stage 4: This stage is added to the flight sequence to improve the robustness of this guidance scheme. The propulsion system is powered off: $u(t) = 0, T_3 \leq t \leq T_4$. The Jacobi integral satisfies $J(t) = J_{\min}$, and τ_4 is an undetermined parameter.

Stage 5: This stage is used to decelerate the spacecraft and increase the Jacobi integral until $J_f = C_1$, which is designed to satisfy the lunar capture condition. The thrust direction is $\alpha = -v/\|v\|$. The flight time τ_5 satisfies

$$C_1 - J(T_f) = C_1 - J_{\min} = \int_{T_4}^{T_4+\tau_5} \frac{2T_{\max}}{m} v dt \tag{24}$$

Note that τ_5 can be determined from τ_2, τ_3 , and τ_4 .

4 Lunar capture set theory and its proof

By using the proposed guidance law in Sect. 3, the dynamics equation of the LTEM spacecraft can be converted into an initial value problem of a differential equation with three parameters, τ_2, τ_3 , and τ_4 .

$$\begin{cases} \dot{s} = f(s) + g(v, m, \tau_2, \tau_3, \tau_4) \\ s(T_0) = s_0, \end{cases} \quad T_0 \leq t \leq T_f \tag{25}$$

The solution of (24) can be denoted as $\varphi(s_0; \tau_2, \tau_3, \tau_4)$ and is determined by the initial state s_0 and τ_2, τ_3, τ_4 . To construct and prove the LCSTs, lemmas regarding the continuity of $\varphi(s_0; \tau_2, \tau_3, \tau_4)$ are presented.

4.1 Lemmas

Lemma 1 *The state of $\varphi(s_0; \tau_2, \tau_3, \tau_4)$ at time T_3 is a continuous function of parameter T_3 .*

Proof The state of $\varphi(s_0; \tau_2, \tau_3, \tau_4)$ at time T_3 can be written as

$$s(T_3) = \int_{T_0}^{T_3} [f(s) + g(v, m, T_2, T_3, T_4)] dt \tag{26}$$

Because $f(s) \in C^1[T_0, T_f]$ is a first-order continuous derivable function, $f(s)$ satisfies the Lipschitz condition, that is, for any $s, \bar{s} \in [T_0, T_5]$,

$$\|f(s) - f(\bar{s})\| < L \|s - \bar{s}\| \tag{27}$$

Let $\varepsilon > 0$. There exists $0 < \delta < \lambda^*$ such that for any T_3, \bar{T}_3 satisfying $|\bar{T}_3 - T_3| < \delta$, we can take $\bar{T}_3 > T_3$; then

$$\begin{aligned} & \|\bar{s}(\bar{T}_3) - s(T_3)\| \\ &= \left\| \int_{T_3}^{\bar{T}_3} \left(f(\bar{s}) - f(s) + \begin{bmatrix} 0_{3 \times 1} \\ \frac{T_{\max}}{m} \bar{\alpha} \\ 0 \end{bmatrix} \right) dt \right\| \\ &\leq \left\| \int_{T_3}^{\bar{T}_3} (f(\bar{s}) - f(s)) dt \right\| + \left\| \int_{T_3}^{\bar{T}_3} \begin{bmatrix} 0_{3 \times 1} \\ \frac{T_{\max}}{m} \bar{\alpha} \\ 0 \end{bmatrix} dt \right\| \\ &\leq \int_{T_3}^{\bar{T}_3} L \|\bar{s} - s\| dt + c(\ln m(T_3) - \ln m(\bar{T}_3)) \end{aligned} \tag{28}$$

Because

$$m = 1 - \frac{T_{\max}}{c} \Delta T \tag{29}$$

and

$$\begin{aligned} \Delta v &= \int_{T'}^{T''} \frac{T_{\max}}{m} dt = c(\ln m(T') - \ln m(T'')) \\ &> T_{\max}(T'' - T') = T_{\max} \Delta T \end{aligned} \tag{30}$$

we have

$$m \geq 1 - \frac{\Delta v}{c} \tag{31}$$

$$\|\bar{s}(\bar{T}_3) - s(T_3)\| \leq \int_{T_3}^{\bar{T}_3} L \|\bar{s} - s\| dt + \frac{T_{\max}}{c - \Delta v} (\bar{T}_3 - T_3) \tag{32}$$

Therefore, by the Grönwall inequality (Hsu 2013),

$$\begin{aligned} \|\bar{s}(\bar{T}_3) - s(T_3)\| &\leq \frac{T_{\max}}{c - \Delta v} (\bar{T}_3 - T_3) \exp\left(\int_{T_3}^{\bar{T}_3} L dt\right) \\ &\leq \frac{T_{\max}}{c - \Delta v} (\bar{T}_3 - T_3) e^{L(\bar{T}_3 - T_3)} \end{aligned} \tag{33}$$

Because $(\bar{T}_3 - T_3)e^{L(\bar{T}_3 - T_3)}$ is a continuous nonnegative function and increases monotonically, there exists λ^* such that $\frac{T_{\max}}{c - \Delta v} \lambda^* e^{L\lambda^*} = \varepsilon$. Therefore,

$$\|\bar{s}(\bar{T}_3) - s(\bar{T}_3)\| < \varepsilon \tag{34}$$

□

Lemma 2 *Solution $\varphi(s_0; \tau_2, \tau_3, \tau_4)$ is a continuous function of T_3 .*

Proof (1) When $T_0 \leq t \leq T_3$, the conclusion holds.

(2) When $T_3 < t \leq T_4$, we have

$$\begin{aligned} \bar{s}(t) &= \bar{s}(\bar{T}_3) + \int_{\bar{T}_3}^t f(\bar{s})dt \\ s(t) &= s(\bar{T}_3) + \int_{\bar{T}_3}^t f(s)dt \end{aligned} \tag{35}$$

Let $\varepsilon > 0$. From Lemma 1, there exists $\delta_1 > 0$, such that

$$\|\bar{s}(\bar{T}_3) - s(\bar{T}_3)\| < \frac{\varepsilon}{2} \tag{36}$$

From the initial value continuous dependence, there exists $\delta_2 > 0$ such that

$$\left\| \int_{\bar{T}_3}^t (f(\bar{s}) - f(s))dt \right\| < \frac{\varepsilon}{2} \tag{37}$$

Then, there exists $\delta = \min(\delta_1, \delta_2)$ such that

$$\begin{aligned} \|\bar{s}(t) - s(t)\| &\leq \|\bar{s}(\bar{T}_3) - s(\bar{T}_3)\| + \left\| \int_{\bar{T}_3}^t (f(\bar{s}) - f(s))dt \right\| \\ &< \varepsilon \end{aligned} \tag{38}$$

(3) When $T_4 < t \leq T_5$, we have

$$\begin{aligned} \bar{s}(t) &= \bar{s}(T_4) + \int_{T_4}^t [f(\bar{s}) + \mathbf{g}(\bar{v}, \bar{m}, T_2, \bar{T}_3, T_4)]dt \\ s(t) &= s(T_4) + \int_{T_4}^t [f(s) + \mathbf{g}(v, m, T_2, T_3, T_4)]dt \end{aligned} \tag{39}$$

Let $\varepsilon > 0$. From (2), there exists $\delta_1 > 0$ such that

$$\|\bar{s}(T_4) - s(T_4)\| < \frac{\varepsilon}{2} \tag{40}$$

From the initial value continuous dependence, there exists $\delta_2 > 0$ such that

$$\begin{aligned} \left\| \int_{T_4}^t \{ [f(\bar{s}) + \mathbf{g}(\bar{v}, \bar{m}, T_2, \bar{T}_3, T_4)] \right. \\ \left. - [f(s) + \mathbf{g}(v, m, T_2, T_3, T_4)] \} dt \right\| < \frac{\varepsilon}{2} \end{aligned} \tag{41}$$

Then, there exists $\delta = \min(\delta_1, \delta_2)$ such that

$$\|\bar{s}(t) - s(t)\| < \varepsilon \tag{42}$$

Thus, the conclusion holds. □

Lemma 3 *Solution $\varphi(s_0; \tau_2, \tau_3, \tau_4)$ is a continuous function of the parameters T_1, T_2 and T_4 .*

The proof of Lemma 3 is similar to that given above.

Corollary 1 *Solution $\varphi(s_0; \tau_2, \tau_3, \tau_4)$ is a continuous function of the parameters τ_2, τ_3 and τ_4 .*

Proof Because $\tau_i = T_i - T_{i-1}$, $i = 2, 3, 4$ are continuous functions, from Lemma 3, the conclusion holds. □

4.2 Lunar capture set theories

As mentioned in Sect. 3, the lunar capture conditions for the LTEM are $J_f = C_1$ and $x|_{L_1} < R_f < x|_{L_2}$. Because $J_f = C_1$ can be satisfied by choosing an appropriate initial value of τ_2 , which causes the transfer trajectories to cross the near- L_1 space, the condition $x|_{L_1} < R_f < x|_{L_2}$ is discussed here by proposing and proving the LCSTs.

LCST 1 Considering the dynamics system in (25) for given parameters $\tau_3 > 0$, $\tau_4 \geq 0$, if $\bar{\tau}_2 \geq 0$ causes the trajectory to satisfy $R_f > x|_{L_2}$, and $\underline{\tau}_2 \geq 0$ causes the trajectory to satisfy $R_f < x|_{L_1}$, there exists $\underline{\tau}_2 < \tau_2^* < \bar{\tau}_2$ satisfying $x|_{L_1} < R_f < x|_{L_2}$.

Proof From Corollary 1, $\varphi(s_0; \tau_2, \tau_3, \tau_4)$ is a continuous function of the parameter τ_2 . Therefore, $R_f = \sqrt{x_f^2 + y_f^2}$ is also a continuous function of τ_2 . According to the definition of continuous functions, there exists $\underline{\tau}_2 < \tau_2^* < \bar{\tau}_2$ satisfying $x|_{L_1} < R_f < x|_{L_2}$. □

LCST 2 Considering the dynamics system in (25), if the parameters $\tau_2 \geq 0$, $\tau_3 > 0$, $\tau_4 \geq 0$, make the trajectory satisfy $R_f > x|_{L_2}$, there exists $0 < \tau_3^* < \tau_3$ satisfying $x|_{L_1} < R_f < x|_{L_2}$.

Proof When $\tau_3 = 0$, the minimum Jacobi integral is $J_{\min} = J(T_2) = C_1$. Therefore, for any $t \in [T_0, T_f]$, $R(t) < x|_{L_1}$. Because there exist $\tau_2 \geq 0$, $\tau_3 > 0$, $\tau_4 \geq 0$ such that $R_f > x|_{L_2}$, and R_f is a continuous function of τ_3 , there exists $0 < \tau_3^* < \tau_3$ satisfying $x|_{L_1} < R_f < x|_{L_2}$. □

LCST 3 Considering the dynamics system in (25), for the parameters $\tau_2 > 0$, $\tau_3 \geq 0$, if $\bar{\tau}_4 \geq 0$ makes the trajectory satisfy $R_f > x|_{L_2}$, and $\underline{\tau}_4 \geq 0$ makes the trajectory satisfy $R_f < x|_{L_1}$, there exists $\underline{\tau}_4 < \tau_4^* < \bar{\tau}_4$ satisfying $x|_{L_1} < R_f < x|_{L_2}$.

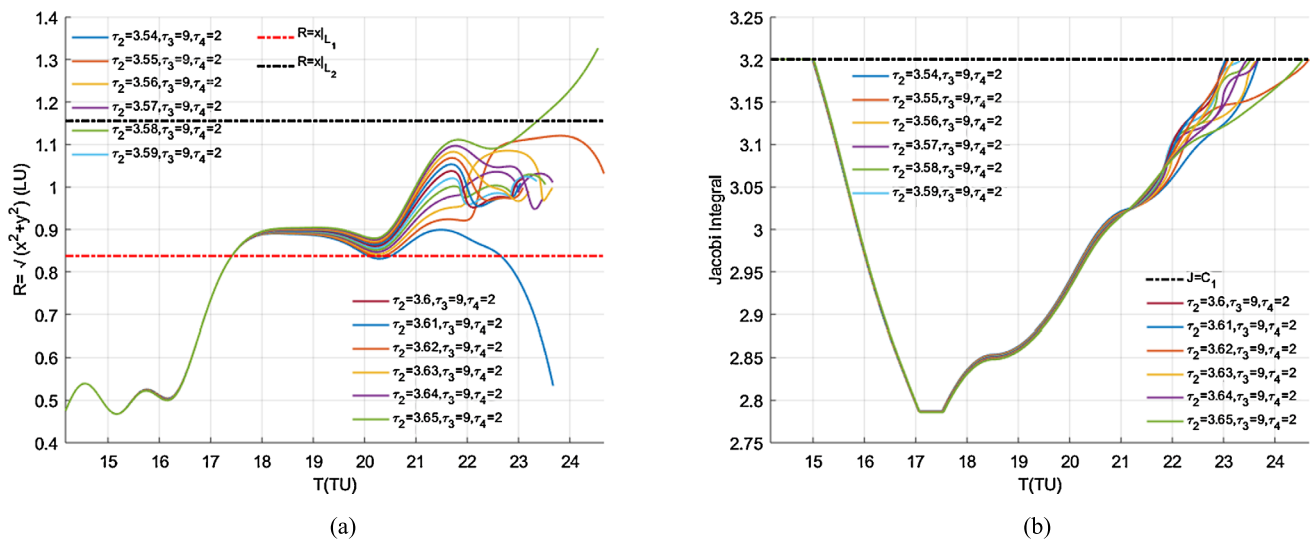


Fig. 4 Variation in (a) $R(t)$, $T_2 \leq t \leq T_f$ and (b) Jacobi integral with τ_2

Proof The process is similar to the proof of LCST 1. \square

LCSTs 1, 2, and 3 involve τ_2 , τ_3 , τ_4 , respectively. It is indicated that if the transfer trajectory whose terminal state has $R_f < x|_{L_1}$ and the transfer trajectory satisfies $R_f > x|_{L_2}$ can be found, then the trajectories satisfying $x|_{L_1} < R_f < x|_{L_2}$ can be obtained. In fact, the transfer trajectories satisfying $R_f < x|_{L_1}$ or $R_f > x|_{L_2}$ can be found more easily than the LTEM T trajectories.

5 Results and discussion

To test the proposed guidance law and the LCSTs, three LTEM T cases with different thrust accelerations are considered. The LTEM T trajectories extend from a geosynchronous orbit with an altitude of approximately 35,827 km to the vicinity of the Moon, where the lunar capture condition is satisfied. The initial mass of the spacecraft is 1,500 kg. Maximum thrusts of 0.45, 0.3, and 0.15 N are considered, and the specific impulse is 3,000 s. The optimal solutions of the last two cases have been discussed in a previous study (Oshima and Campagnola 2017) and provide a basis for comparison of the results. In the previous study, a global search for LTEM Ts in the planar CRTBP was conducted, and the minimum-fuel LTEM T trajectories were computed using an indirect method. Therefore, the optimal solutions in the literature provide the lower limit of fuel consumption for the planar LTEM T. The fourth/fifth-order Runge–Kutta method, with the relative and absolute tolerances set to 10^{-13} , was used to integrate Eq. (21). All the cases were analyzed using a computer with a 3.30 GHz, four-core i5 processor and 4 GB of onboard memory.

5.1 First case study

In the first case study, we determine the LTEM T trajectories for a thrust of 0.45 N ($3 \times 10^{-4} \text{ m/s}^2$) and a cut-off value of $\eta_{cut} = 0$. The initial parking orbit has an inclination of 28.5° with respect to the Moon orbit. The initial right ascension of the ascending node and true anomaly are 80° and 280° , respectively.

First, an initial value of the parameter τ_2 is iteratively computed by viewing the projection of the transfer trajectory onto the x – y plane of the Earth–Moon rotating frame to satisfy the condition that the spacecraft can cross the near- L_1 space. This step requires eight iterations, which take 57.67 s. Then, the transfer trajectories whose terminal states satisfy $R_f < x|_{L_1}$ and $R_f > x|_{L_2}$ can easily be found. Finally, the lunar capture sets for τ_2 , τ_3 , τ_4 are solved by searching between the parameters of the above two trajectories on the basis of the LCSTs. At the same time, the parameters of the minimum-fuel LTEM T trajectory can be found; this takes several seconds, because it does not include the numerical integration in stage 1, which accounts for most of the computational cost.

Figures 4–6 present the variation in $R(t)$ and $J(t)$ in the transfer trajectories. The unit of τ is days. On the left side, the curves with terminal states located at $x|_{L_1} < R_f < x|_{L_2}$ and Jacobi integrals equal to C_1 , represent the LTEM T trajectories. Figure 4 shows the variation in $R(t)$ and $J(t)$ during $T_2 \leq t \leq T_f$ for $\tau_2 \in [3.54, 3.65]$, $\tau_3 = 9$, and $\tau_4 = 2$. It can be seen that $J_f = C_1$ is held for all the options in Fig. 4(b). When $\tau_2 = 3.65$, then $R_f > x|_{L_2}$, and when $\tau_2 = 3.54$, then $R_f < x|_{L_1}$. Then, from LCST 1, there exists $\tau_2 \in (3.54, 3.65)$ such that $x|_{L_1} < R_f < x|_{L_2}$. Finally, the lunar capture set of $\tau_2 \in [3.55, 3.64]$, $\tau_3 = 9$, and $\tau_4 = 2$ is found for the LTEM T trajectory. Figure 7 shows the LTEM T

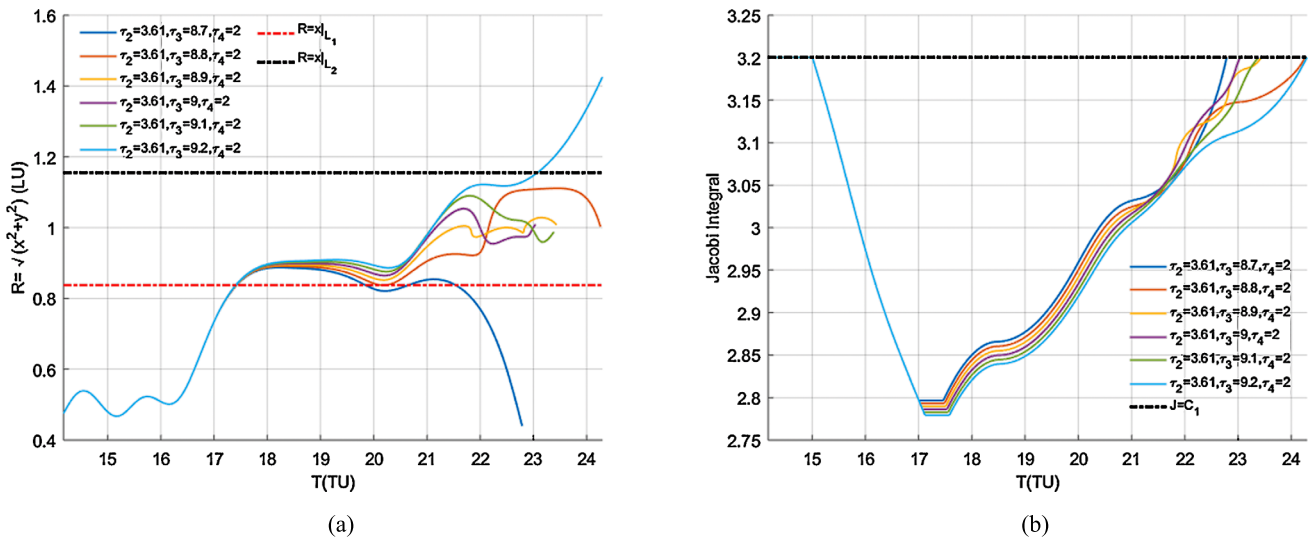


Fig. 5 Variation in (a) $R(t)$, $T_2 \leq t \leq T_f$ and (b) Jacobi integral with τ_3

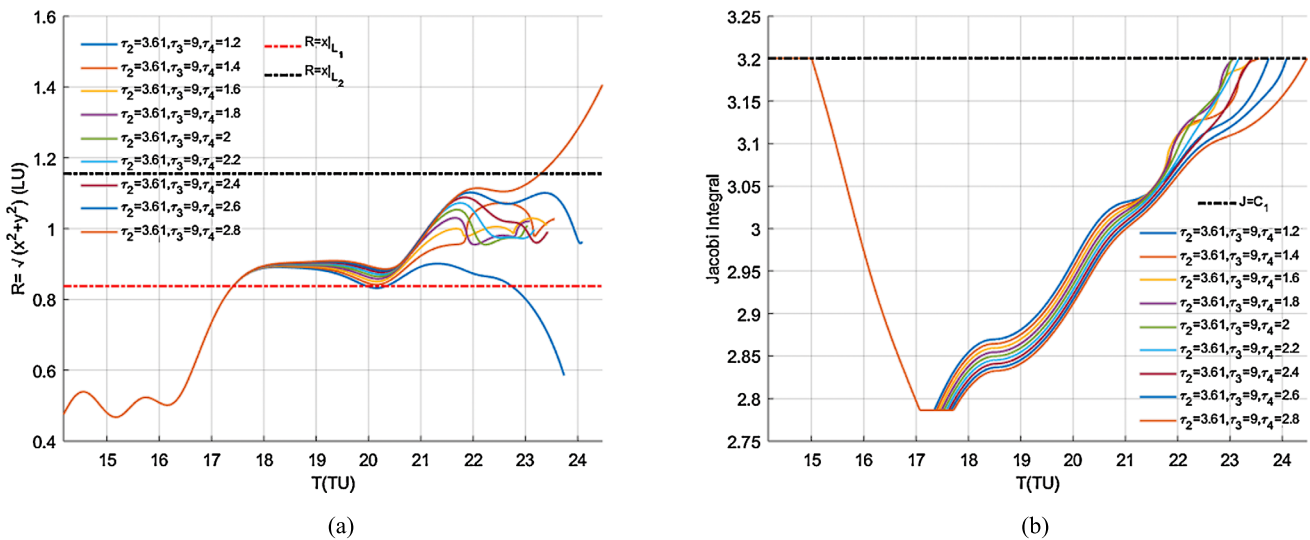


Fig. 6 Variation in (a) $R(t)$, $T_2 \leq t \leq T_f$ and (b) Jacobi integral with τ_4

trajectory with $\tau_2 = 3.61$, $\tau_3 = 9$, and $\tau_4 = 2$. The total flight time is 100.18 days, and the corresponding fuel cost is 124.98 kg, which is equivalent to a final-to-initial mass ratio of 0.9167. The total computational cost for finding the lunar capture set is 66.12 s.

Figure 5 shows the variation in $R(t)$ and $J(t)$ with $T_2 \leq t \leq T_f$ for parameters $\tau_2 = 3.61$, $\tau_3 \in [8.7, 9.2]$, and $\tau_4 = 2$. When $\tau_3 = 9.2$, then $R_f > x|_{L_2}$, and when $\tau_3 = 8.7$, then $R_f < x|_{L_1}$. Then, from LCST 2 and the numerical calculation, $\tau_2 = 3.61$, $\tau_3 \in [8.8, 9.1]$, and $\tau_4 = 2$ is the lunar capture set that generates the LTEM T trajectories. Figure 6 shows that, for $\tau_2 = 3.61$ and $\tau_3 = 9$, there exists $\tau_4 \in [1.3, 2.6]$, which satisfies the lunar capture condition from LCST 3.

5.2 Second case study

In the second case, planar LTEM Ts are established with a thrust of 0.3 N (2×10^{-4} m/s²) and cut-off values of 0.1, 0.2, 0.3, 0.4, and 0.5.

As in the first case, τ_2 is solved iteratively. The number of iterations is related to the preset cut-off values. More iterations are needed for larger cut-off values. For example, when $\eta_{cut} = 0.1$, at most three iterations are needed, which take 130.14 s, but when $\eta_{cut} = 0.5$, it takes seven iterations and 547.61 s to find the parameter. Then, lunar capture sets for τ_2, τ_3, τ_4 are obtained by searching the parameter intervals determined by the LCSTs. During this process, the minimum-fuel LTEM T trajectories are obtained.

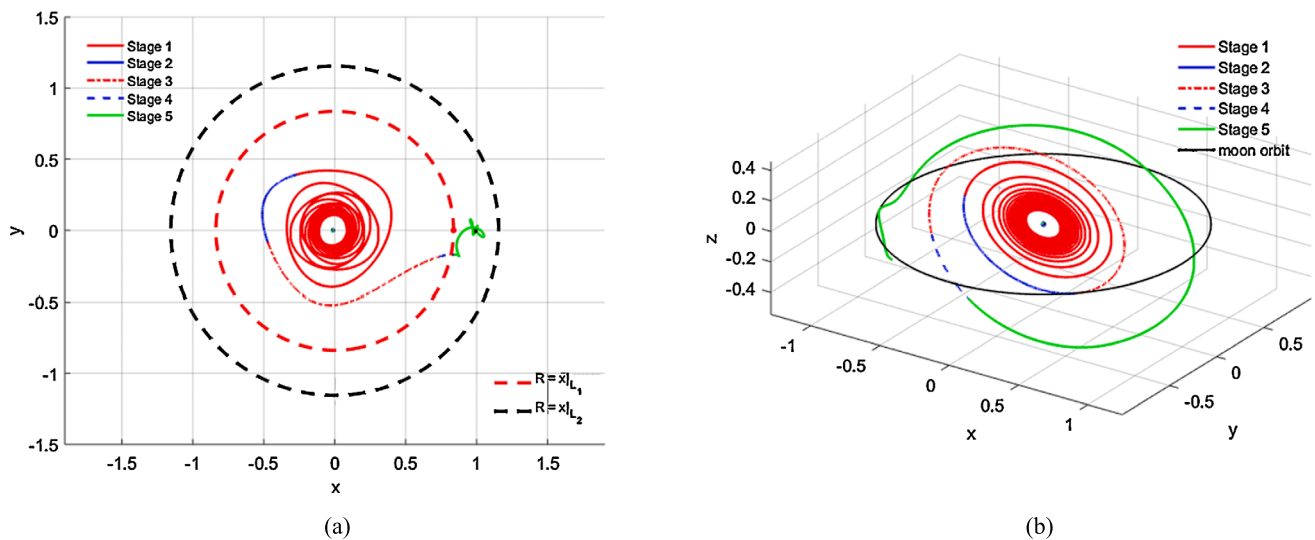


Fig. 7 LTEM T trajectory in (a) Earth–Moon rotating frame (projection on the x – y plane) and (b) Earth-centered inertial frame

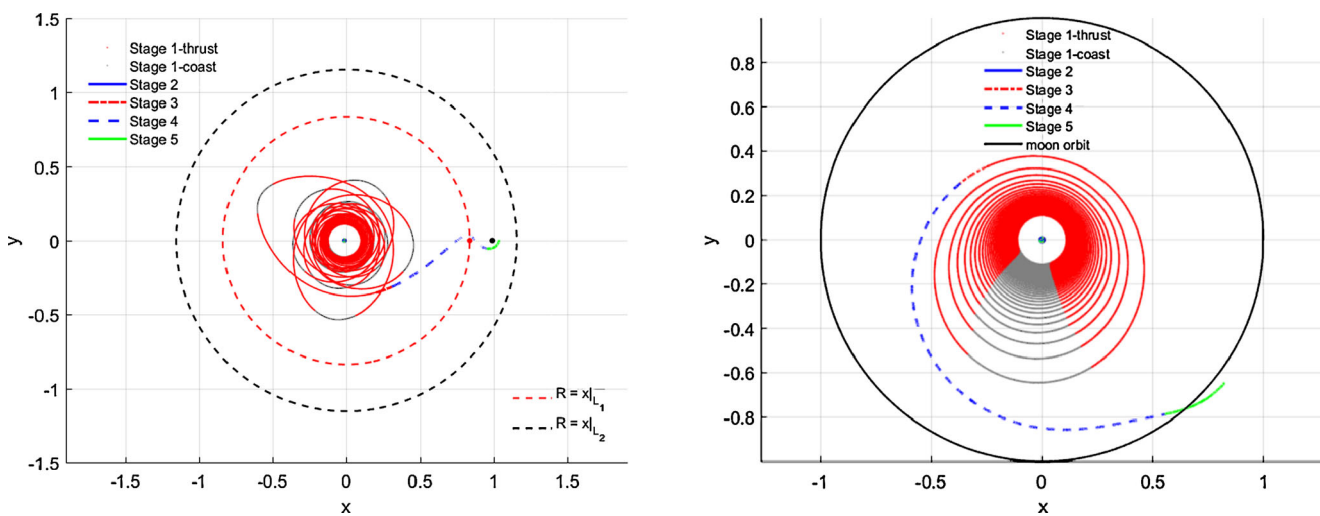


Fig. 8 Minimum-fuel LTEM T trajectory for a thrust of 0.3 N and $\eta_{cut} = 0.1$

Figures 8–12 show the minimum-fuel LTEM T trajectories for different η_{cut} in both the Earth–Moon rotating frame (left) and the Earth-centered inertial frame (right). The LTEM T trajectories have five stages, as described in Sect. 3.4. The red lines or dots represent the acceleration propulsion segments, where $u = 1$ and $\alpha = v/v$. The green lines represent the deceleration segments, where $u = 1$ and $\alpha = -v/v$. The blue lines represent the coast segments, where $u = 0$. The gray dots represent the states where the thrust efficiency is below η_{cut} . As shown on the left, the terminal states of the transfer trajectories are located in areas where $x|_{L_1} < R_f < x|_{L_2}$, indicating that the trajectories satisfy the lunar capture condition. The figures on the right-hand side show that for larger cut-off values of the thrust efficiency, the thrust is more concentrated near perigee.

The corresponding parameters are listed in Table 3 for various η_{cut} . Here, ΔT is the flight time, and Δm is the fuel consumption. The computation time is the computational cost of searching for τ_2, τ_3, τ_4 for the lunar capture sets and minimum-fuel solutions. As indicated in Table 3, for larger cut-off values of the thrust efficiency, the flight time is longer, and less fuel is consumed. The search can be completed in several seconds, because it does not include the numerical integration over Stage 1, which accounts for most of the calculation time.

The optimal solutions of this case reported in Oshima and Campagnola (2017) provide a basis for comparison of the results, as shown in Table 3. Here, Δm_{opt} is the optimal fuel consumption. The fuel consumption obtained in this paper is comparable with (at most 2.52% higher than) the optimal

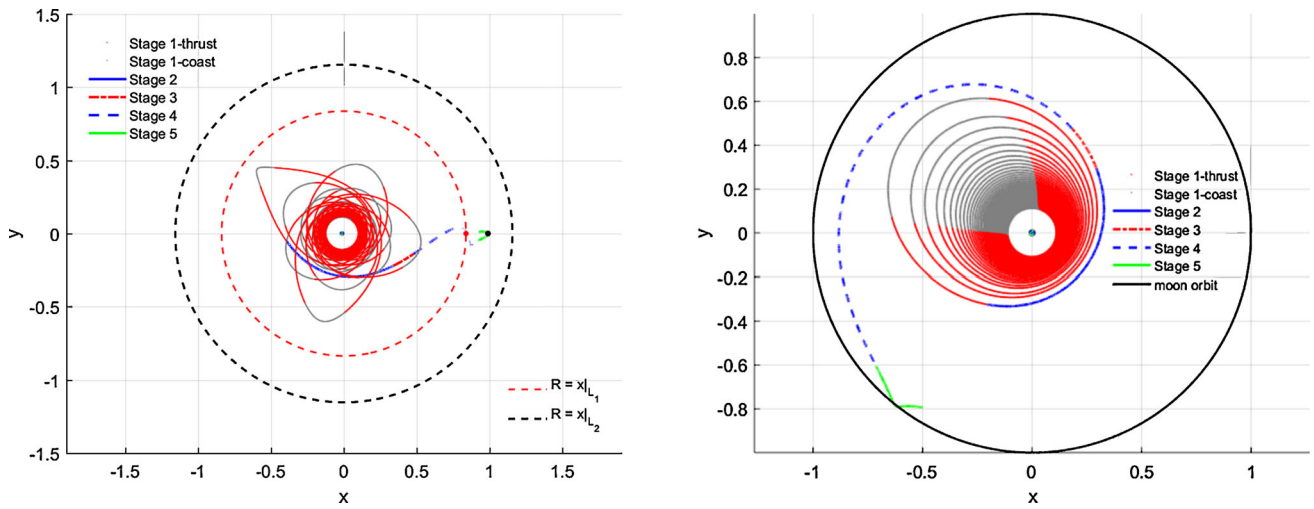


Fig. 9 Minimum-fuel LTEM trajectory for a thrust of 0.3 N and $\eta_{cut} = 0.2$

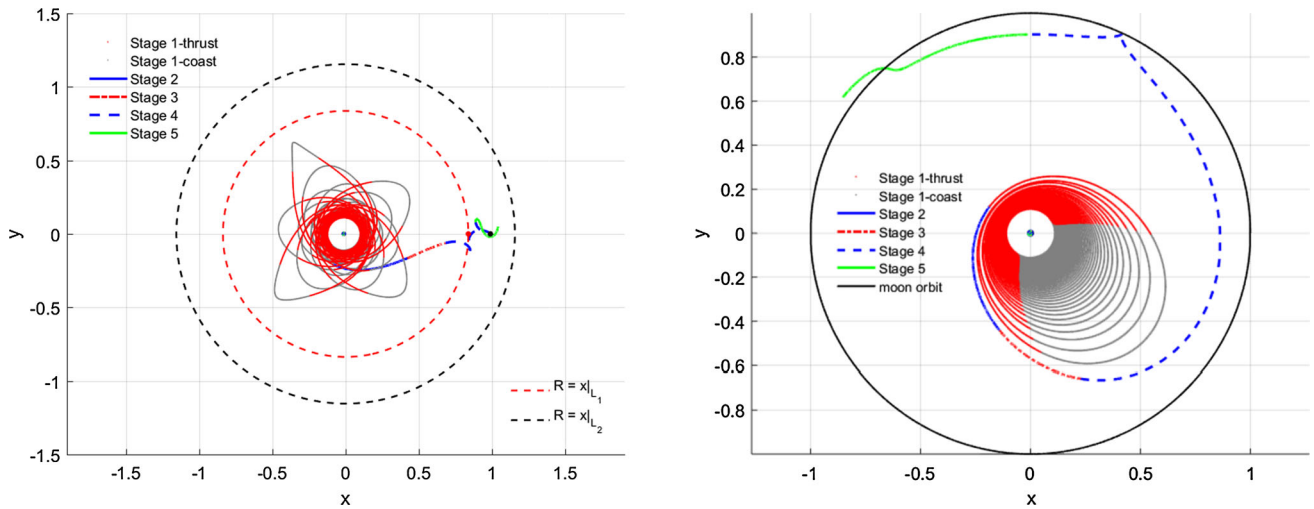


Fig. 10 Minimum-fuel LTEM trajectory for a thrust of 0.3 N and $\eta_{cut} = 0.3$

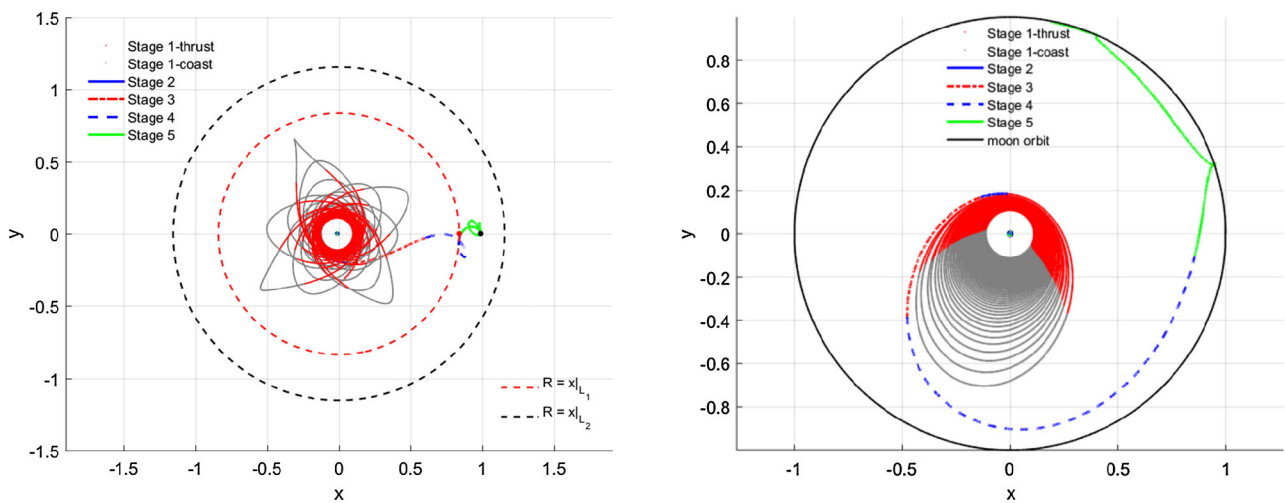


Fig. 11 Minimum-fuel LTEM trajectory for a thrust of 0.3 N and $\eta_{cut} = 0.4$

value. In terms of the computational cost, although a three-dimensional set was also searched, the numerical integration over all of the LTEM T trajectories is not negligible. Thus, the computational cost of the LCST-based solutions is relatively low compared with that of the referenced solutions in the literature.

5.3 Third case study

In the third case, planar LTEM T trajectories are determined for a thrust of 0.15 N and η_{cut} values of 0.1, 0.2, 0.3, 0.4, and 0.5. The maximum thrust in this case is half that in the second case, and the initial acceleration is only 1×10^{-4} m/s².

Similarly, τ_2 is solved iteratively. Because the thrust acceleration is half that in the second case, the numerical integration time for a single iteration is relatively long. For $\eta_{cut} = 0.1$, it takes at most three iterations and 242.79 s to solve the parameter. For $\eta_{cut} = 0.5$, it takes seven iterations and 16.8 min to obtain the initial value of τ_2 . Then, the lunar capture sets and minimum-fuel LTEM T trajectories are found by searching over the parameter intervals determined by the LCSTs.

The minimum-fuel LTEM T trajectories in both the Earth–Moon rotating frame (left) and the Earth-centered inertial frame (right) are shown in Figs. 13–17. The terminal states in the figures (left side) are located in the regions where $x|_{L_1} < R_f < x|_{L_2}$, indicating that the states satisfy the lunar capture condition. Consistent with the flight control sequence, five stages are included in the LTEM T trajectories. The gray dot in the figures on the right side represents the position where the thrust efficiency is smaller than the preset η_{cut} . The figures indicate that when the cut-off value is large, most of the thrust is concentrated near perigee.

The corresponding parameters of the minimum-fuel LTEM T trajectories with different preset η_{cut} values are reported in Table 4. As expected, at larger cut-off values of the thrust efficiency, the flight time is longer, and the fuel consumption is lower. A comparison of the obtained fuel consumption values with the optimal values in Oshima and Campagnola (2017) shows that the trajectories are comparable with (at most 1.88% higher than) the optimal solutions. Table 4 also lists the computation time required to search for τ_2, τ_3, τ_4 . The computational cost is only tens of seconds.

6 Robustness analysis

In this section, the robustness of the guidance law based on the LCSTs is demonstrated by considering the navigation and switching time τ_i ($i = 2, 3, 4$) errors.

6.1 Navigation error

In the actual flight mission, the thrust direction and velocity in the Earth–Moon rotating frame deviate owing to navigation error. It is assumed that uncorrelated, unbiased Gaussian errors, characterized by $\sigma_{pos} = 5$ km and $\sigma_{vel} = 5$ m/s, are applied to simulate the navigation error of the position (subscript pos) and velocity (subscript vel), respectively (D’Souza et al. 2007).

One thousand Monte Carlo simulations of the nominal LTEM T trajectory with $\tau_2 = 0$, $\tau_3 = 0.4$, and $\tau_4 = 9$ in the second case study were performed. As shown in Fig. 18(a), all the terminal states satisfy the lunar capture condition $x|_{L_1} < R_f < x|_{L_2}$, where $x|_{L_1} = 0.83736$ and $x|_{L_2} = 1.15527$. Thus, the LCST-based guidance law is robust with respect to the navigation errors. The flight time of the nominal LTEM T trajectories with navigation errors ranges from 133.59 to 135.41 days, and the fuel cost is increased by at most 1.58 kg, as shown in Fig. 18(b).

6.2 Switching time error

This section shows the importance of the LCSTs when there are errors in the switching times T_2, T_3, T_4 . To maintain consistency with Sect. 5, τ_2, τ_3, τ_4 are used instead of T_2, T_3, T_4 .

In the first case study, the lunar capture sets based on the LCSTs were found. Table 5 shows the lunar capture sets for the nominal LTEM T trajectories in the second and third case studies. The results show that the switching times have a relatively wide range of values. For example, in the first case study for $\eta_{cut} = 0.1$, the flight time of Stage 2 can range from 0 to 0.6 days, the flight time of Stage 3 can range from 0.3 to 2.1 days, and the flight time of Stage 4 varies over a period of more than 10 days. The LCSTs are used to find feasible sets of τ_2, τ_3, τ_4 that satisfy the lunar capture condition. Therefore, the LCST-based LTEM T trajectories are robust with respect to the switching time.

Additionally, there are a number of other key points with regard to the method itself. First, the approach focuses on lunar capture. Therefore, any LTEM Ts in the lunar capture set ensure that the spacecraft can be captured by the Moon. Second, compared with other methods in which the thrust direction is solved using nonlinear optimization by the direct method or using the two-point boundary value problem for optimal control by the indirect method, the proposed method is based on a relatively simple guidance law, in which the thrust direction is the same as or opposite to the velocity in the Earth–Moon rotating frame. Therefore, it is practical for engineering implementations.

7 Conclusion

This study investigates the LTEM T trajectories by exploring the lunar capture set. Based on the CRTBP, the sufficient

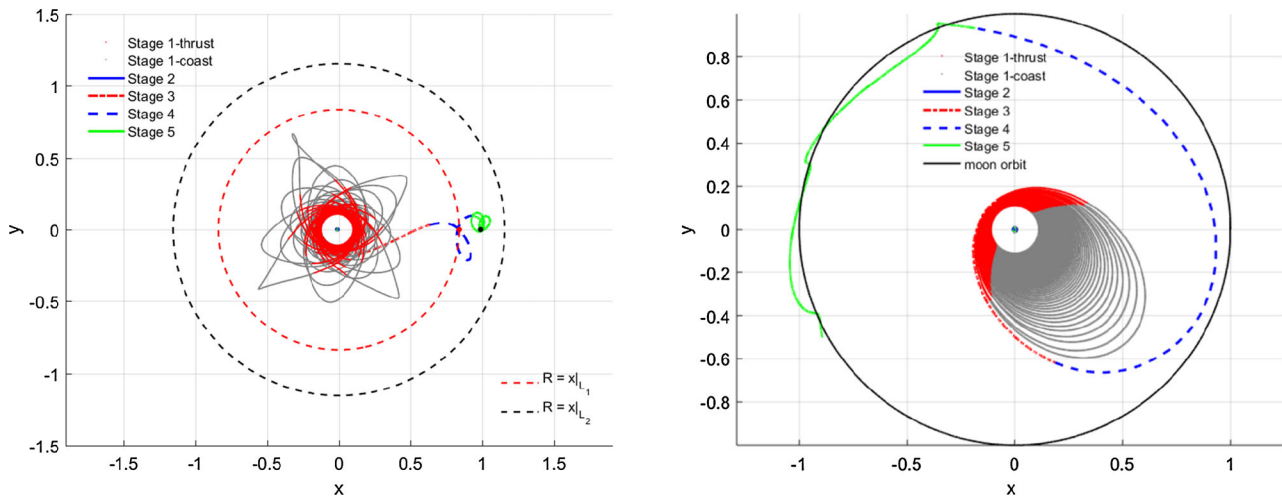


Fig. 12 Minimum-fuel LTEM trajectory for a thrust of 0.3 N and $\eta_{cut} = 0.5$

Table 3 Parameters of the minimum-fuel LTEM trajectories for a thrust of 0.3 N

η_{cut}	τ_2 (day)	τ_3 (day)	τ_4 (day)	ΔT (day)	Δm (kg)	Δm_{opt} (kg)	Computation time (s)
0.1	0	0.4	9	133.69	82.84	81.25	33.68
0.2	2.1	0.6	10.5	154.59	78.12	77.48	45.64
0.3	1.1	1.3	10	171.86	74.73	73.33	81.34
0.4	0.2	1.8	10.0	196.89	72.57	71.25	100.56
0.5	0	2.3	13	234.27	70.96	69.17	91.65

Table 4 Parameters of the minimum-fuel LTEM trajectories for a thrust of 0.15 N

η_{cut}	τ_2 (day)	τ_3 (day)	τ_4 (day)	ΔT (day)	Δm (kg)	Δm_{opt} (kg)	Computation time (s)
0.1	0.3	0.4	13	261.74	82.32	80.77	59.22
0.2	0.3	0.7	8.5	289.68	77.58	76.67	70.01
0.3	0.2	1	11	332.11	73.88	73.33	86.86
0.4	0.1	1.4	10.5	382.78	70.74	–	116.71
0.5	0.1	2.2	12	448.34	67.73	66.53	130.04

Table 5 Lunar capture sets for LTEM trajectories with switching time errors

Case	η_{cut}	τ_2, τ_3, τ_4 (day)	τ_2, τ_3, τ_4 (day)	τ_2, τ_3, τ_4 (day)
Second case study	0.1	[0, 0.6], 0.4, 9	0, [0.3, 2.1], 9	0, 0.4, [5, 25]
	0.2	[0, 2.2], 0.6, 10.5	2.1, [0.6, 1.2], 10.5	2.1, 0.6, [4, 11]
	0.3	[0.9, 1.1], 1.3, 10	1.1, [1.3, 1.5], 10	1.1, 1.3, [5, 25]
	0.4	[0.1, 0.2], 1.8, 10	0.2, [1.7, 2.0], 10	0.2, 1.8, [5, 18]
	0.5	[0, 0.02], 2.3, 13	0, [2.3, 2.4], 13	0, 2.3, [6, 20]
Third case study	0.1	[0, 0.3], 0.4, 13	0.3, [0.4, 0.7], 13	0.3, 0.4, [6, 18]
	0.2	[0, 1.9], 0.7, 8.5	1, [0.5, 1.1], 8.5	1, 0.7, [5, 20]
	0.3	[0.1, 0.2], 1, 11	0.2, [0.96, 1.05], 11	0.2, 1, [5, 20]
	0.4	[0, 0.4], 1.4, 10.5	0.1, [1.34, 1.47], 10.5	0.1, 1.4, [5, 20]
	0.5	[0, 0.2], 2.2, 12	0.1, [2.2, 2.3], 12	0.1, 2.2, [5, 20]

condition for lunar capture is given on the basis of the Jacobi integral and Hill’s region. A guidance law including the thrust direction, the thrust efficiency, and a five-stage flight

control sequence is proposed. Then, an initial value problem of an ordinary differential equation with three parameters is obtained. Through a proof of the continuity of the three

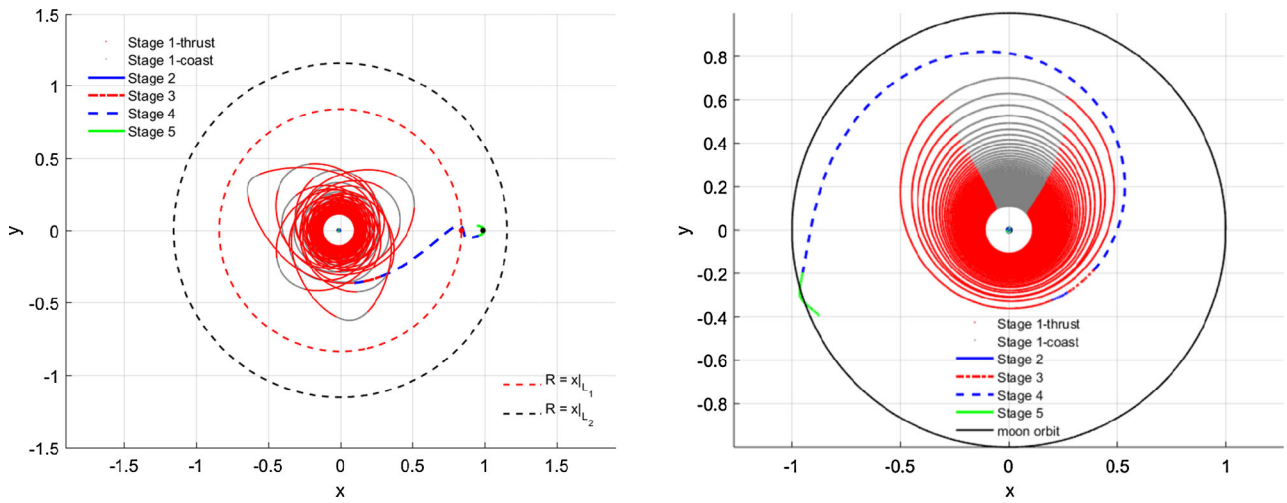


Fig. 13 Minimum-fuel LTEM trajectory for a thrust of 0.15 N and $\eta_{cut} = 0.1$

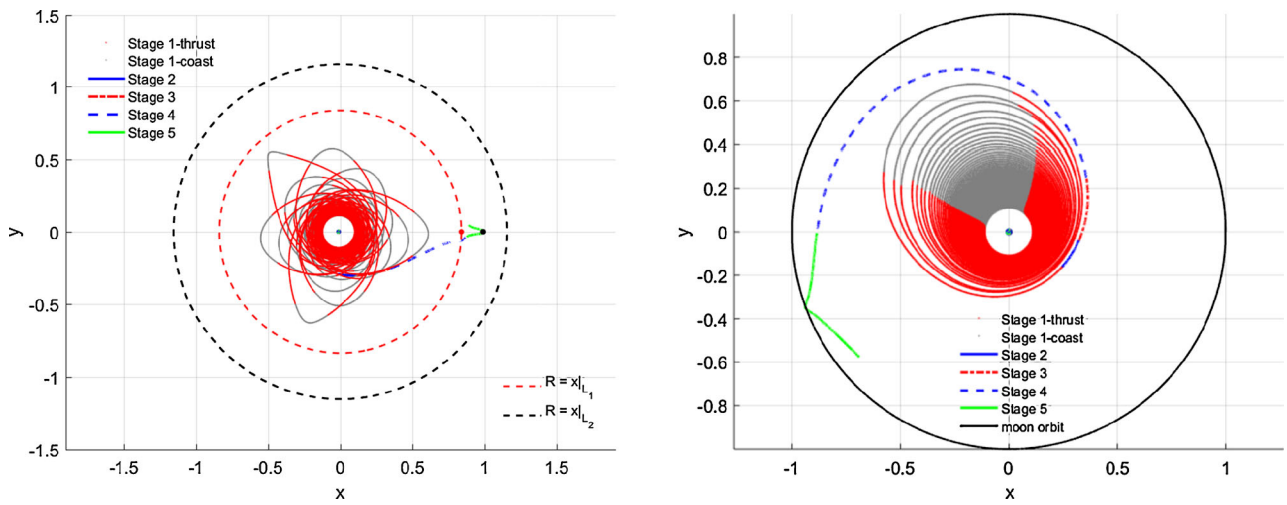


Fig. 14 Minimum-fuel LTEM trajectory for a thrust of 0.15 N and $\eta_{cut} = 0.2$

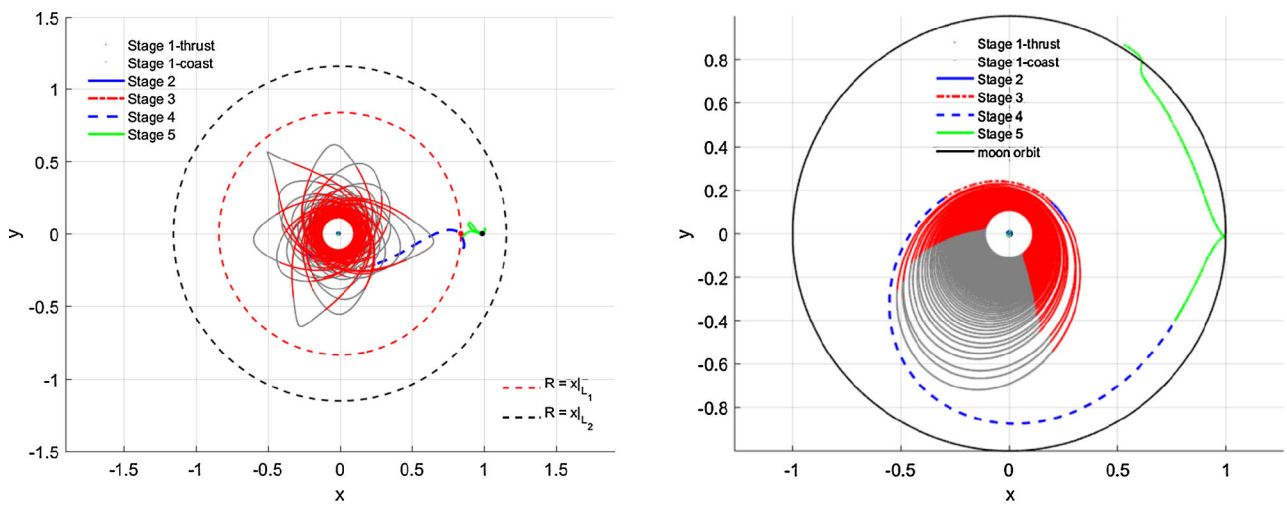


Fig. 15 Minimum-fuel LTEM trajectory for a thrust of 0.15 N and $\eta_{cut} = 0.3$

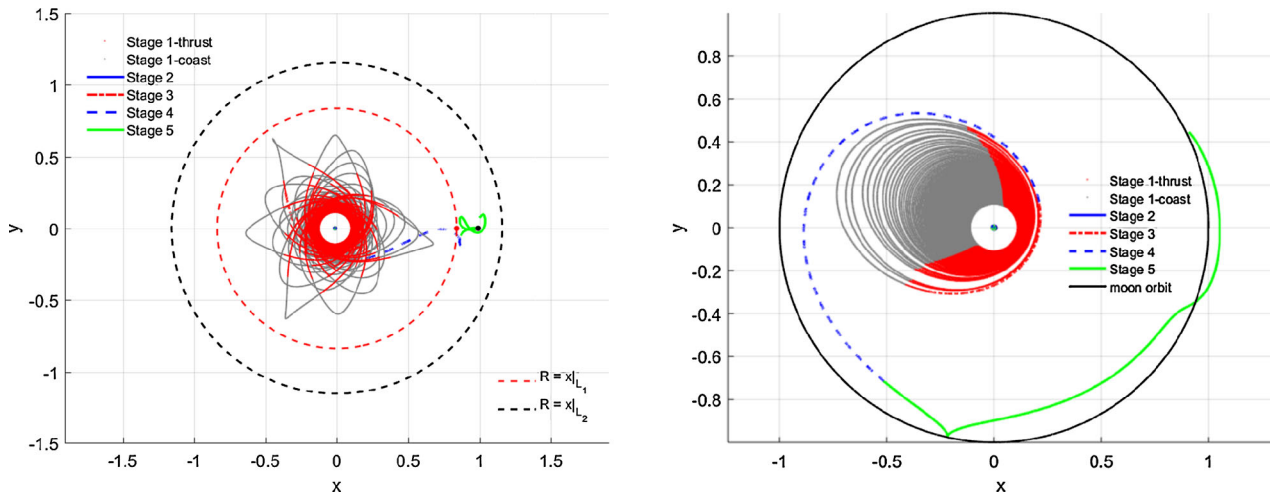


Fig. 16 Minimum fuel LTEM trajectory for a thrust of 0.15 N and $\eta_{cut} = 0.4$

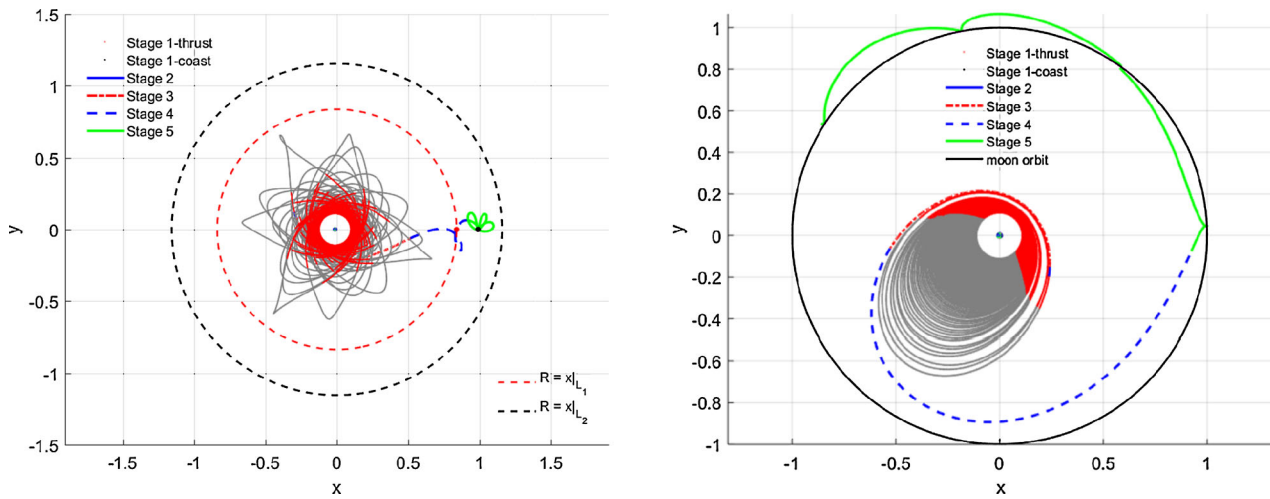


Fig. 17 Minimum-fuel LTEM trajectory for a thrust of 0.15 N and $\eta_{cut} = 0.5$

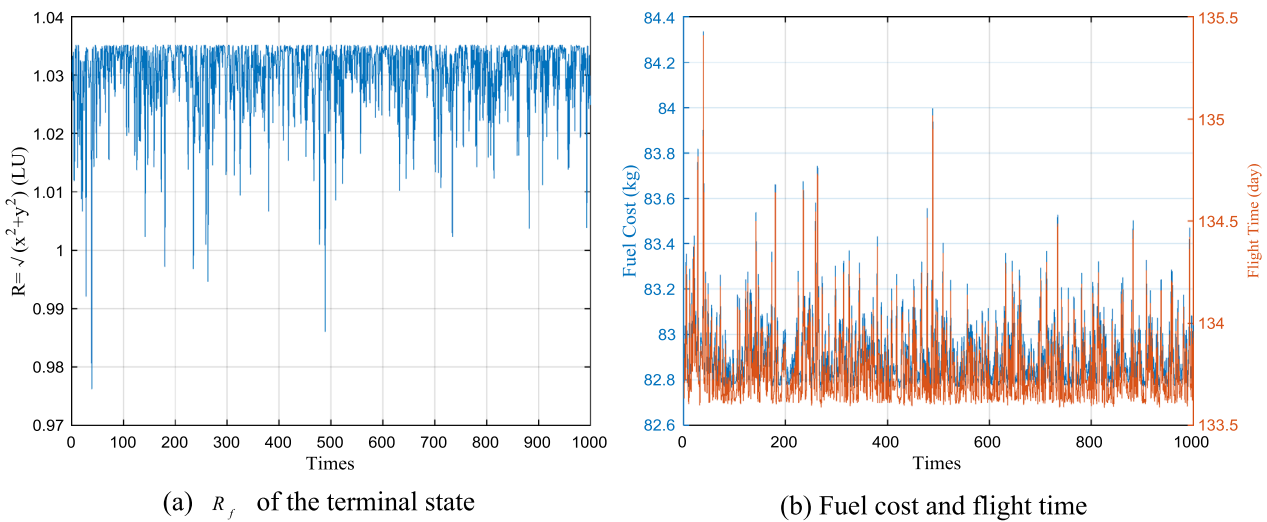


Fig. 18 Results of Monte Carlo simulations of the nominal trajectory with $\eta = 0.1$ in the second case study

parameters, the LCSTs are proposed and proved; they can greatly simplify the LTEMPT trajectory design.

The lunar capture sets and corresponding LTEMPT trajectories departing from a geosynchronous orbit with an altitude of approximately 35,827 km for different thrust accelerations and preset cut-off values can be easily determined from the LCSTs. The resulting LTEMPT trajectories are comparable to the optimal solutions. The robustness is analyzed to show the adaptability of the proposed method assuming navigation and switching time errors. The results show that the LCSTs proposed in this paper are significant for the generation of lunar capture sets and can provide technical support for future cislunar cargo spacecraft.

Acknowledgement This research was supported by the National Natural Science Foundation of China (no. 11572168 and 11872034).

Publisher's Note Springer Nature remains neutral with regard to jurisdictional claims in published maps and institutional affiliations.

References

- Betts, J.T.: Survey of numerical methods for trajectory optimization. *J. Guid. Control Dyn.* **21**(2), 193–206 (1998). <https://doi.org/10.2514/2.4231>
- Betts, J.T., Erb, S.O.: Optimal low thrust trajectories to the Moon. *SIAM J. Appl. Dyn. Syst.* **2**(2), 144–170 (2003). <https://doi.org/10.1137/S1111111102409080>
- Caillau, J.B., Daoud, B., et al.: Minimum fuel control of the planar circular restricted three-body problem. *Celest. Mech. Dyn. Astron.* **114**, 137–150 (2012). <https://doi.org/10.1007/s10569-012-9443-x>
- Chi, Z.M., Li, H.Y., et al.: Power-limited low-thrust trajectory optimization with operation point detection. *Astrophys. Space Sci.* **363**, 122 (2018). <https://doi.org/10.1007/s10509-018-3344-8>
- Chi, Z.M., Yang, H.W., et al.: Homotopy method for optimization of variable-specific-impulse low-thrust trajectories. *Astrophys. Space Sci.* **362**, 216 (2017). <https://doi.org/10.1007/s10509-017-3196-7>
- Crusan, J.C., Smith, R.M., et al.: Deep space gateway concept: extending human presence into cislunar space. In: 2018 IEEE Aerospace Conference, Big Sky, MT, 3–10 March (2018). <https://doi.org/10.1109/AERO.2018.8396541>
- D'Souza, C., Crain, T., et al.: In: Orion Cislunar Guidance and Navigation, AIAA Guidance, Navigation and Control Conference and Exhibit, Hilton Head, South Carolina, 20–23 August (2007). <https://doi.org/10.2514/6.2007-6681>
- Gao, Y.F., Wang, Z.K., et al.: Analytical design methods for transfer trajectories between the Earth and the Lunar Orbital Station. *Astrophys. Space Sci.* **363**, 206 (2018). <https://doi.org/10.1007/s10509-018-3426-7>
- Gao, Y.: Earth–Moon trajectory optimization using solar electric propulsion. *Chin. J. Aeronaut.* **20**, 452–463 (2007). [https://doi.org/10.1016/s1000-9361\(07\)60067-3](https://doi.org/10.1016/s1000-9361(07)60067-3)
- Graham, K.F., Rao, A.V.: Minimum-time trajectory optimization of multiple revolution low-thrust Earth-orbit transfers. *J. Spacecr. Rockets* **52**(3), 289–303 (2015). <https://doi.org/10.2514/1.A33187>
- Graham, K.F., Rao, A.V.: Minimum-time trajectory optimization of low-thrust Earth-orbit transfers with eclipsing. *J. Guid. Control Dyn.* **53**(2), 711–727 (2016). <https://doi.org/10.2514/1.A33416>
- Haberkorn, T., Martinon, P.: Low-thrust minimum-fuel orbital transfer: a homotopic approach. *J. Guid. Control Dyn.* **27**(6), 1046–1060 (2004). <https://doi.org/10.2514/1.4022>
- Herman, A.L., Conway, B.A.: Optimal low-thrust Earth–Moon orbit transfer. *J. Guid. Control Dyn.* **21**(1), 141–147 (1998). <https://doi.org/10.2514/2.4210>
- Hoffman, D.J., Kerslake, T.W., et al.: Concept Design of High Power Solar Electric Propulsion Vehicles for Human Exploration. NASA/TM-2011-217281 (2011)
- Hsu, S.B.: Ordinary Differential Equations with Applications, pp. 33–34. World Scientific, Singapore (2013). ISBN-13: 978-9814452908
- Jagannatha, B.B., Bouvier, J.H., et al.: Preliminary design of low-energy, low thrust transfers to halo orbits using feedback control. *J. Guid. Control Dyn.* **42**, 2 (2018). <https://doi.org/10.2514/1.G003759>
- Jiang, F.H.: Practical techniques for low-thrust trajectory optimization with homotopic approach. *J. Guid. Control Dyn.* **35**(1), 245–257 (2012). <https://doi.org/10.2514/1.52476>
- Kluever, C.A., Pierson, B.L.: Optimal low-thrust three-dimensional Earth–Moon trajectories. *J. Guid. Control Dyn.* **18**(4), 830–837 (1995). <https://doi.org/10.2514/3.21466>
- Lee, D.H., Bang, H., et al.: Efficient initial costates estimation for optimal spiral orbit transfer trajectories design. *J. Guid. Control Dyn.* **32**(6), 1943–1947 (2009). <https://doi.org/10.2514/1.44550>
- Lee, D.H., Bang, H., et al.: Optimal Earth–Moon trajectory design using new initial costate estimation method. *J. Guid. Control Dyn.* **35**(5), 1671–1675 (2012). <https://doi.org/10.2514/1.55863>
- Mammarella, M., Vernicari, P.M., et al.: How the Lunar Space Tug can support the cislunar station. *Acta Astronaut.* **154**, 181–194 (2019). <https://doi.org/10.1016/j.actaastro.2018.04.032>
- McGuire, M.L., Burke, L.M., et al.: Low thrust cis-lunar transfers using a 40 kw-class. In: Solar Electric Propulsion Spacecraft, AAS/AIAA Astrodynamics Specialist Conference 2017, Stevenson, WA, August (2017)
- Mengali, G., Quarta, A.A.: Optimization of biimpulsive trajectories in the Earth–Moon restricted three-body system. *J. Guid. Control Dyn.* **28**(2), 209–216 (2005). <https://doi.org/10.2514/1.7702>
- Mercer, C.R., McGuire, M.L., et al.: Solar Electric Propulsion Concepts for Human Space Exploration. NASA/TM-2016-218921 (2016). <https://doi.org/10.2514/6.2015-4521>
- Oshima, K., Campagnola, S.: Global search for low-thrust transfers to the Moon in the planar circular restricted three-body problem. *Celest. Mech. Dyn. Astron.* **128**, 303–322 (2017). <https://doi.org/10.1007/s10569-016-9748-2>
- Ozimek, M.T., Howell, K.C.: Low-thrust transfers in the Earth–Moon system, including applications to libration point orbits. *J. Guid. Control Dyn.* **33**(2), 533–549 (2010). <https://doi.org/10.2514/1.43179>
- Pan, B.F., Pan, X., et al.: A new probability-one homotopy method for solving minimum-time low-thrust orbital transfer problems. *Astrophys. Space Sci.* **363**, 198 (2018). <https://doi.org/10.1007/s10509-018-3420-0>
- Pérez-Palau, D., Epenoy, R.: Fuel optimization for low-thrust Earth–Moon transfer via indirect optimal control. *Celest. Mech. Dyn. Astron.* **130**, 21 (2018). <https://doi.org/10.1007/s10569-017-9808-2>
- Petropoulos, A.E., Longuski, J.M.: Shape-based algorithm for automated design of low-thrust, gravity-assist trajectories. *J. Spacecr. Rockets* **41**(5), 787–796 (2004). <https://doi.org/10.2514/1.13095>
- Pierson, B.L., Kluever, C.A.: Three-stage approach to optimal low-thrust Earth–Moon trajectories. *J. Guid. Control Dyn.* **17**(6), 1275–1282 (1994). <https://doi.org/10.2514/3.21344>
- Song, Y.J., Park, S.Y.: A lunar cargo mission design strategy using variable low thrust. *Adv. Space Res.* **43**, 1391–1406 (2009). <https://doi.org/10.1016/j.asr.2009.01.020>

- Taheri, E., Abdelkhalik, O.: Fast initial trajectory design for low-thrust restricted-three-body problems. *J. Guid. Control Dyn.* **38**(11), 2146–2160 (2015). <https://doi.org/10.2514/1.G000878>
- Taheri, E., Abdelkhalik, O.: Initial three-dimensional low-thrust trajectory design. *Adv. Space Res.* **57**, 889–903 (2016). <https://doi.org/10.1016/j.asr.2015.11.034>
- Taheri, E., Kolmanovsky, I.: Shaping low-thrust trajectories with thrust-handling feature. *Adv. Space Res.* **61**, 879–890 (2018). <https://doi.org/10.1016/j.asr.2017.11.006>
- Woolley, R.G., Baker, J.D., et al.: Cargo logistics for a notional Mars base using solar electric propulsion. *Acta Astronaut.* **156**, 51–57 (2019). <https://doi.org/10.1016/j.actaastro.2018.08.026>
- Zhang, C., Toppoto, F., et al.: Low-thrust minimum-fuel optimization in the circular restricted three-body problem. *J. Guid. Control Dyn.* **38**(8), 1501–1509 (2015). <https://doi.org/10.2514/1.G001080>